ON THE INFLUENCE OF ADVECTION COOLING DURING DEGRADATION AND REGENERATION OF BORON-OXYGEN DEFECTS USING HIGH INTENSITIES

Axel Herguth, Alexander Graf, Giso Hahn
University of Konstanz, Department of Physics
PO Box 676, 78457 Konstanz, Germany

ABSTRACT: For the industrial application of the regeneration treatment to mitigate boron-oxygen related light-induced degradation (BO-LID), the process has to work in just a few seconds. Fortunately, the regeneration process (including both degradation and the actual regeneration phase) can be sped up by both higher charge carrier injection and temperature to fulfill this requirement. Unfortunately, there is an upper temperature limit due to reverse reactions, and higher injection comes at the price of unwanted heating. Hence, it is on the one hand of utmost importance to find measures to keep temperature below a certain threshold while increasing injection by illumination. On the other hand, a quick heat-up into a certain temperature range is required to bring process times down to the second range. Within this contribution, it is shown that temperature and illumination intensity can be decoupled to a certain degree thanks to advection cooling, and how a smart control of high intensity laser illumination and advection cooling can further reduce process times.
Keywords: LID, regeneration, heat management

1 INTRODUCTION

The occurrence of boron-oxygen related light-induced degradation (BO-LID) of bulk lifetime [1,2], especially in crystalline silicon grown by Czochralski's method (Cz-Si), poses a problem to the development of highly efficient solar cells based on p-type crystalline silicon wafers which generally implies a better usage of high bulk lifetimes by better surface passivation, *e.g.* [3].

Fortunately, the negative impact of BO-LID can be permanently mitigated by an illuminated annealing treatment also known as regeneration [4-6], during which BO related defects are passivated. Generally speaking, illuminated annealing first leads to the formation of the harmful BO-related defects (degradation reaction) and afterwards to their passivation (regeneration reaction). Both reactions, degradation as well as regeneration, can be accelerated by increasing temperature and injection (by illumination) [1,2,7-9]. However, there are reverse reactions to be taken into account as well which accelerate with temperature, too [1,2,5]. Hence, temperature and injection are the relevant 'adjustment screws' to adjust the required process times for nowadays mass production.

As demonstrated, *e.g.*, in [5,10], completeness of regeneration is more and more compromised when temperature during illuminated annealing exceeds a certain threshold temperature which depends on cell properties and injection conditions. This threshold temperature implies a minimal process duration that can only be undercut in exchange for a less complete regeneration. Increasing injection raises this threshold temperature allowing for higher process temperatures and thus shorter durations without sacrificing regeneration completeness.

Hence, there is an optimum temperature range where required duration is sufficiently short but temperature is still low enough to suppress reverse reactions. Whether high illumination intensity is a wise choice, depends crucially on heat management or, in other words, on the perfect balance of heating and cooling allowing for a fast heat-up phase on the one hand and, on the other hand, the avoidance of excessive heating despite high intensities.

Within this contribution, the impact of advection cooling on sample temperature is investigated and optimization strategies are discussed.

2 EXPERIMENTAL SETUP

In order to provide a well-controlled environment for the advection cooling experiments, a wind tunnel has been constructed that is schematically depicted in Fig. 1. The $5 \times 5\,\mathrm{cm}^2$ sample is integrated in an air channel of ~3 mm in height and 55 mm in width, so that the sample virtually seals the channels off and acts more or less as a seamless continuation of the wall. Electronically controlled fans press/suck air through the channel allowing for a variation of air speed. Hence, advection cooling only applies to the rear side of the sample. The channel is designed to provide a mostly laminar air flow underneath the sample. Heat transfer from sample to air perpendicular to the air flow is expected to extend only a few millimeters, meaning that air flowing laminar in a distance of more ~3 mm would not contribute much to actual heat removal anyway.

The planar silicon sample, doped with $\sim 7 \cdot 10^{15}\,\mathrm{cm}^{-3}$ and coated by ~75 nm SiN_x:H ($n \sim 2.0$ at 600 nm), is illuminated from above with a homogenized 805 nm laser with adjustable intensity. No significant temperature difference between sample front side, where laser absorption predominantly heats the sample, and rear side, where advection cooling takes effect, is expected simply because heat conductivity of the thin (~155 µm) silicon sample is very high with $\sim 100\,\mathrm{W/cm^2/K}$. Hence, even a heat flux of $\sim 100\,\mathrm{W/cm^2}$ between front to rear would yield only a small temperature difference of 1 K.

The temperature of the sample is monitored optically from above by a thermal camera which is sensitive in the 7-14 µm range (LWIR). It is important to note here that within this range, free charge carriers play a major role for the optical properties of silicon (cp. collective oscillations of the electron plasma, plasma frequency, Drude model).

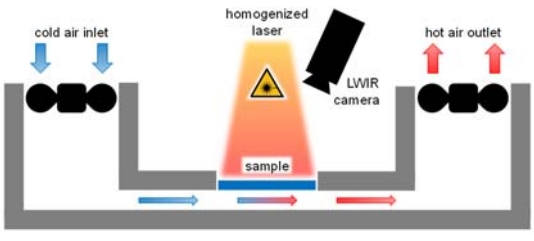

Figure 1: Cross-section drawing of the used wind tunnel.

This especially impacts the thermal emission coefficient ε which is a key parameter for the optical measurement of temperature. How strongly a change in charge carrier density due to light absorption impacts the optical 'raw' temperature measurement is demonstrated in Fig. 2. While the laser intensity of ~20 suns (j_{sc} equivalent, [11]) is switched on and off with 1 Hz, raw temperature of the LWIR camera is monitored. As can be seen, there is a large step in raw temperature of ±60°C when charge carriers are generated or vanish by recombination within a few milliseconds. This deviation in raw temperature depends not only on excess charge carrier density (thus the product of laser power density and effective lifetime) but on actual sample temperature as well as it is shown in Fig 3. This large discrepancy has to be taken into account by calibrating the camera signal accordingly. It is interesting to note from Fig. 2 as well that, while the camera observes an increase/decrease of ±10°C, the thermocouple, which is attached to the rear side of the sample, does not exactly reproduce these changes. Most probably, the thermocouple is either too thermally inert to follow the fast modulation of laser intensity or the thermal coupling to the sample is insufficient. Either way, the thermocouple is not suitable to monitor the fast temperature changes seen later on, even though it shows a general upward trend indicating that the system is still adjusting its mean temperature to the modulation. In the following, temperatures measured by the LWIR camera are corrected for each laser intensity similar to the described approach in Fig. 2 and Fig. 3.

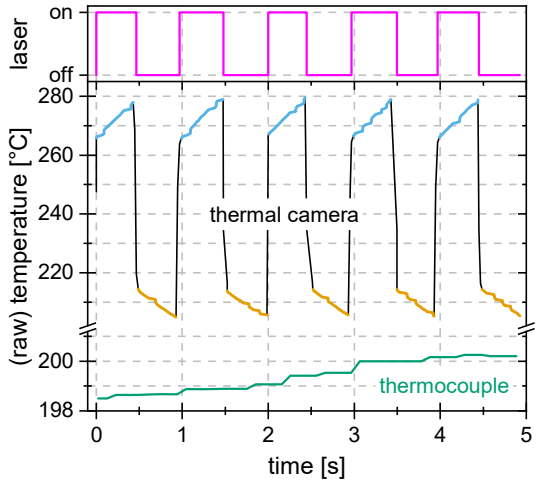

Figure 2: Non-calibrated raw temperature of the LWIR camera and a thermocouple during pulsed laser operation.

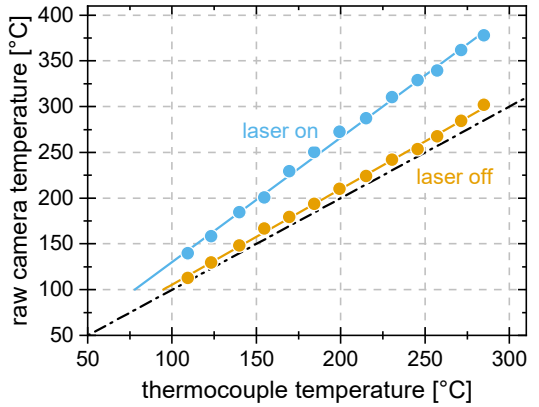

Figure 3: Non-calibrated raw temperature signal versus thermocouple temperature during the laser on and off phases in Fig. 2.

3 RESULTS

One of the major drawbacks of the wind tunnel is exemplarily depicted in Fig. 4. Since the air heats up continuously during the transit underneath the sample, the temperature difference between air and sample decreases along the air flow and less heat is dissipated. Thus cooling is more efficient at the front edge and less efficient at the rear edge of the sample. Then, however, the temperature further down the sample decreases less and less which widens the temperature gap again and leads in turn to stronger cooling. In consequence, the specific design of the wind tunnel results unavoidably in a temperature gradient in the direction of the air flow, whereas there should be none perpendicular to the air flow. While Fig. 4 confirms the first trend apart from a certain edge effect which is probably caused by an unintended air leakage there, the missing top/bottom mirror symmetry shows either an inhomogeneous laser illumination and/or an inhomogeneous air flow.

The asymmetry in flow direction is also illustrated as cross-sectional view in Fig. 5 for different air speeds. While maximum temperature for vanishing air speed is found in the front part of the sample, advection cooling shifts it to the rear part. Even though the absolute temperature decreases with increasing air speed, the shape is more or less the same for all curves with non-vanishing air speed. In the following, temperature is always averaged in a central 3×3 cm^2 region to cancel out edge effects.

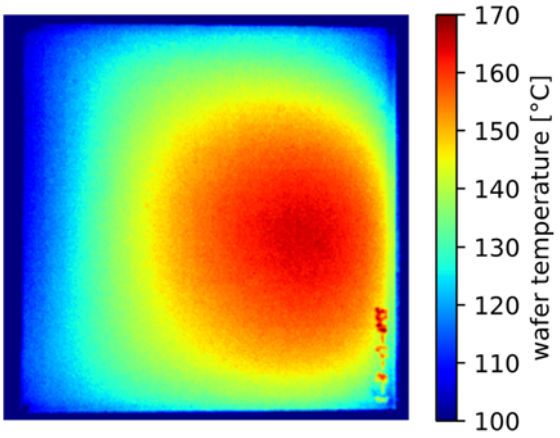

Figure 4: Equilibrium temperature distribution within a 5×5 cm^2 sample illuminated with 20 suns and cooled with an air speed of 8 m/s.

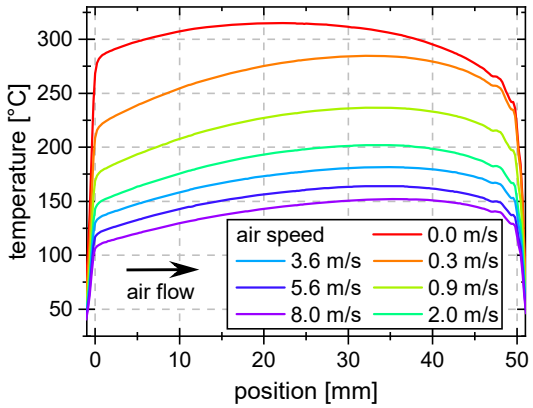

Figure 5: Cross-sectional equilibrium temperature profiles for an illumination intensity of 20 suns and different air speeds.

In order to quantify the impact of advection cooling on sample temperature, different air speeds are used while laser intensity is kept constant. The resulting temperature profiles are exemplarily shown for 20 suns (j_{sc} equivalent, [11]) in Fig. 6. At this point it is not the aim to reach a short process duration, but to quantify the key aspects like maximum temperatures and cooling rates. Therefore, the illumination time was chosen to 30 s which is sufficient to reach maximum temperature.

Figure 7 shows the cooling rates extracted from Fig. 6 during the cool-down phase. As can be seen, the cooling rates depend approximately linearly on the sample temperature almost across the whole data range and cross at the temperature at which the air is blown into the wind tunnel. Hence, cooling rate scales with the difference between sample and blown-in air temperature. Only at high sample temperatures reached for low air speed the cooling rate becomes super-linear probably due to radiative cooling according to Stefan-Boltzmann's law (dash-dotted line).

The linear dependence of the cooling rate on the difference of actual temperature T and room temperature T_0 allows to describe the temporal dynamic system by the continuity equation (conservation of power)

$$\Delta P = c \cdot \frac{dT}{dt} = P_{\text{laser}} - k \cdot (T - T_0) \qquad (1)$$

in which the difference between incoming power P_{laser} of the laser and (predominantly) advection cooling is buffered in the sample with heat capacity c. The ratio k/c corresponds to the negative slope of the cooling curves in Fig. 7 and depends on air speed. The solution of the differential equation is given by

$$T(t) = T_0 + \frac{P_{\text{laser}}}{k} \cdot \left[1 - \exp\left(-\frac{k}{c} \cdot t\right)\right] \qquad (2)$$

Thus the ratio k/c determines how long it takes to reach a certain fraction of the long-term equilibrium temperature

$$T(\infty) = T_0 + \frac{P_{\text{laser}}}{k} \qquad (3)$$

Two consequences arise from that:

(i) As lower air speeds result in flatter and flatter slopes and thus smaller k-values, it takes longer and longer to approach the long-term equilibrium temperature as can be seen in Fig. 6.

(ii) The lower k-value of low air speeds result in higher long-term equilibrium values as $T(\infty)$ scales inversely with k as can be seen in Fig. 6.

The cooling rates (k/c) exemplarily extracted at 75°C are shown in the top part of Fig. 8 and the obtained maximum temperatures $T(\infty)$ in the bottom part of Fig. 8. It is noteworthy that Eq. 3 can be used to determine the incident laser power confirming the direct measurements of laser intensity with a reference solar cell.

As can be seen from Fig. 8, cooling rate scales sub-linearly with air speed. Hence one can conclude that efficient cooling becomes more difficult, the more heat needs to be dissipated. Nevertheless, advection cooling was that effective here that even at 20 suns laser power, a temperature of ~150°C could not be overcome anymore and it allowed to increase laser intensity from 10 to 20 suns while retaining the same sample temperature by increasing air speed from ~0.5 to ~8 m/s.

This demonstrates that sample temperature and intensity can be successfully decoupled to a certain degree thanks to advection cooling.

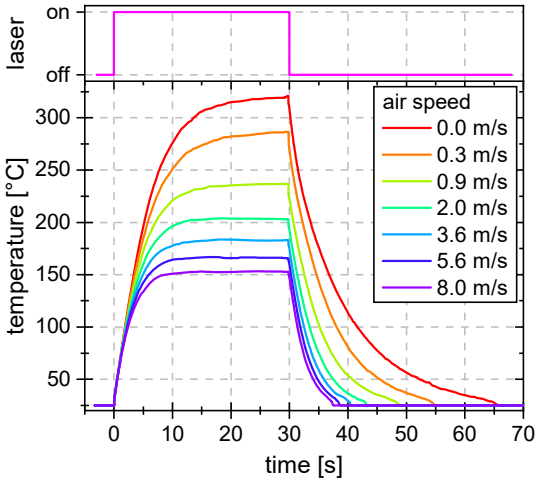

Figure 6: Temperature profiles for different air speeds using a laser intensity of 20 suns (j_{sc} equivalent [11]).

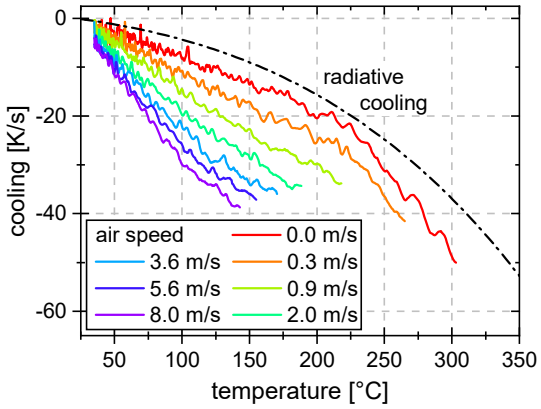

Figure 7: Cooling rates versus temperature extracted from the cool-down ramps of Fig. 6. The dash-dotted line depicts the expected cooling rate for pure radiative cooling assuming ε = 0.7.

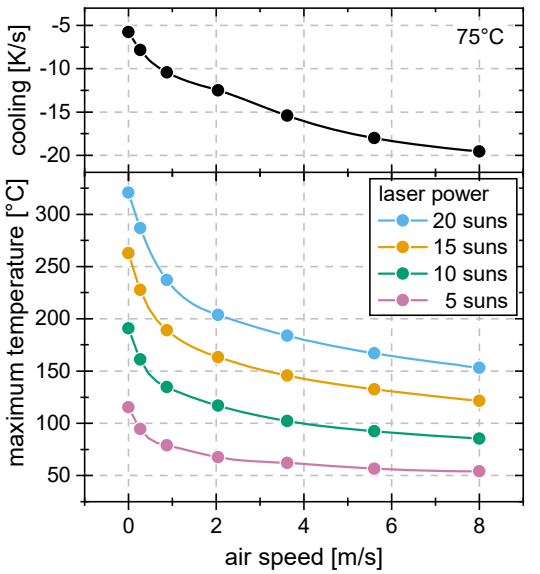

Figure 8: Cooling rates at 75°C (top) and maximum temperatures using different laser intensities (bottom) versus air speed extracted from Fig. 7 and Fig. 6.

4 OPTIMIZATION STRATEGIES

On the one hand, the permanent cooling ensures that the sample target temperature is not exceeded and that the sample quickly cools down afterwards. On the other hand, it also prevents a quick heating up as it is illustrated by the orange curve in Fig. 9 (8.0 m/s curve from Fig. 6). Using a laser intensity of 20 suns, it still takes almost 10 s to bring the sample to the intended temperature which is obviously detrimental to industrially relevant process times. Two solutions for this issue are depicted in Fig. 9 as well.

A first option is to delay the onset of advection cooling so that the sample heats up faster in the beginning without sacrificing temperature control in the subsequent plateau phase and the fast cool-down phase (green line). However, at least in the used setup with fans, switching on the advection cooling does not work instantaneous resulting in a slight temperature overshoot. In addition, even without advection cooling (green dashed line), it takes ~3.5 s to cross the equilibrium temperature.

A second option is to increase laser intensity in the beginning while keeping the advection cooling constant to enforce a quicker heat-up phase. In the depicted calculation (blue line), laser intensity is increased to 100 suns for ~0.6 s before it falls back to 20 suns to quickly retain the target temperature.

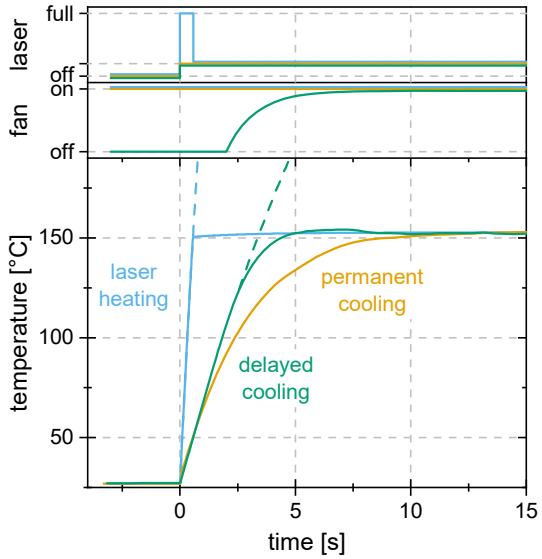

Figure 9: Measured (orange, green) and calculated (blue) temperatures profiles during the heat up phase using 20 suns illumination intensity an ~8 m/s air speed.

ACKNOWLEDGEMENT

Part of this work was supported by the German Federal Ministry of Economic Affairs and Energy under contract numbers 0324080C and 0324001.

The content is the responsibility of the authors.

REFERENCES

[1] K. Bothe, J. Schmidt, Journal of Applied Physics 99 (2006) 013701.

[2] T. Niewelt, J. Schön, W. Warta, S.W. Glunz, M.C. Schubert, IEEE Journal of Photovoltaics 7 (2017) 383.

[3] A. Herguth, AIP Conference Proceedings 2147 (2019) 140004.

[4] A. Herguth, G. Schubert, M. Kaes, G. Hahn, Proceedings 21st European Photovoltaic Energy Conference (2006) 530

[5] A. Herguth, G. Hahn, Journal of Applied Physics 108 (2010) 114509.

[6] B. Hallam, A. Herguth, P. Hamer, N. Nampalli, S. Wilking, M. Abbott, S. Wenham, G. Hahn, Applied Sciences 8 (2018) 10.

[7] V. Steckenreiter, D.C. Walter, J. Schmidt, AIP Advances 7 (2017) 035305.

[8] P. Hamer, B. Hallam, M. Abbott, S. Wenham, Physica Status Solidi (RRL) - Rapid Research Letters 9 (2015) 297

[9] A. Graf, A. Herguth, G. Hahn, AIP Advances 8 (2018) 085219.

[10] A. Herguth, C. Derricks, G. Hahn, Proceedings 33rd European Photovoltaic Energy Conference (2017) 557.

[11] A. Herguth, Energy Procedia 124 (2017) 53.